AIAA JOURNAL
Vol. 38, No. 1, January 2000

Multibody Implementation of Finite Volume C^0 Beams

Gian Luca Ghiringhelli,* Pierangelo Masarati,† and Paolo Mantegazza‡
Politecnico di Milano, 20158 Milan, Italy

A C^0 beam discretization based on the finite volume concept is described. In the linear case this approach leads to a collocated evaluation of the stiffness matrix of the beam; it proves to be intrinsically free from shear locking. In the nonlinear formulation only a collocated evaluation of the elastic forces is required, which dramatically simplifies the computation of the elastic contribution to the equilibrium equations. The formulation is here developed for the general geometrically nonlinear case and implemented in multibody formulation. The proposed approach proved to be consistent; its major drawback lies in the loss of symmetry of both the linear and the linearized beam matrices. For this reason the method is particularly suitable for dynamic problems like a nonlinear implicit multibody numerical approximation, in which the symmetry of the matrices is not so important, as it is already lost, whereas the ease in the generation of the contributions to the equations can lead to faster and cheaper analyses. Some applications are outlined, and the most relevant results are discussed.

Nomenclature

$\mathcal{A}$	= three-node beam element arm matrix, 18×12
D	= beam section linear elastic constitutive matrix, 6×6
$\mathcal{D}$	= three-node beam constitutive matrices at evaluation points, 12×12
$e_i, i = 1, 3$	= orthogonal unit vectors
$\mathcal{F}$	= three-node beam nodal forces and couples, 18×1
$f_i, i = 1, 3$	= offset from node to beam reference point
$G\backslash(Gg')\times = R'R^T$	= differential rotation matrix
g	= modified Gibbs–Rodriguez rotation parameters
$\mathcal{M}$	= beam section inertial matrix
$N_i(\xi), i = 1, 3$	= shape functions
$p : B \subseteq \Re \mapsto \Re^3$	= reference line
q	= multibody nodal degrees of freedom, 9×1
R	= orthonormal rotation matrix
$\mathcal{R}$	= three-node beam rotation matrices at evaluation points, 12×12
T	= differential arm matrix, 6×6
U	= arm matrix, integral of matrix T
$v \equiv \dot{p}$	= velocity
$w(\xi)$	= weight function, unit-valued inside $[a, b]$
$x_i, i = 1, 3$	= position of a node
$\delta(\xi)$	= Dirac's impulse function
Θ	= three-node beam internal forces and moments at evaluation points, 12×12
$\vartheta = \{t, m\}$	= internal forces and moments, 6×1
$\xi \in B$	= curvilinear abscissa on B
$\rho\backslash\rho\times = R'R^T$	= geometric curvature
τ	= distributed forces and couples, 6×1
φ	= arbitrary rotation vector
Ψ	= three-node beam strains and curvatures at evaluation points, 12×1
$\psi = \{\varepsilon, \kappa\}$	= deformations, 6×1: strains and curvatures
$\omega\backslash\omega\times \equiv \dot{R}R^T$	= angular velocity

Received 6 March 1998; revision received 5 May 1999; accepted for publication 11 May 1999. Published by the American Institute of Aeronautics and Astronautics, Inc., with permission.

*Associate Professor (Design of Aerospace Structures), Dipartimento di Ingegneria Aerospaziale, via La Masa 34; ghiringhelli@aero.polimi.it.

†Associate Researcher, Dipartimento di Ingegneria Aerospaziale, via La Masa 34.

‡Full Professor (Aeroelasticity), Dipartimento di Ingegneria Aerospaziale, via La Masa 34.

Introduction

BEAMS are an important tool of structural analysis because they represent a relatively simple model compared to a three-dimensional analysis of slender structural systems. The finite element method found its first applications in structural analysis of trusses and frames; nowadays numerical analysis of beam structures is still important, and beam elements play an important role in almost all commercially available finite element analysis codes. Great efforts have been made by many researchers to improve understanding of beams. The characterization of the elastic behavior of beams has been treated by Giavotto et al.,[1] Bauchau,[2] Hodges et al.,[3] Ghiringhelli and Mantegazza,[4] and Borri et al.,[5] among the others, whereas three-dimensional behavior, with particular regard to dynamic response, has been studied by many, including Bathe and Bolourchi,[6] Borri and Merlini,[7] Simo,[8] Simo and Vu-Quoc,[9] Borri and Bottasso,[10,11] and Ghiringhelli.[12] An important class of beam models is represented by C^0 beams, which remove the simplifying assumption of zero shear deformation that characterizes Euler beams. However such a beam model is known to suffer from shear locking when low-order shape functions are used to interpolate nodal displacements and rotations.[13] The locking can be overcome in many ways, ranging from relaxed integration to hybrid and strain-based formulations.[12] An alternative solution is represented by the proposed method, based on the finite volume concept. Finite volumes are widely used in fields like computational fluid dynamics and heat transfer, whereas their use in structural analysis has been shaded by the diffusion of well-suited variational principles. As already stated, the variational approach is known to suffer from shear locking; the finite volume approximation instead proved to be intrinsically shear lock free.[14] So it is worth exploring the possibility of extending that formulation to geometrically nonlinear beams to be used within multibody formulations, where the loss of symmetry of the stiffness matrix is not important because it is usually already lost because of other contributions.[15,16]

Finite Volume Formulation

Differential Equilibrium Equation

The beam is defined by a regular reference line p that maps the one-dimensional domain B to the three-dimensional space, namely, $p : B \subset \Re \mapsto \Re^3$. The position of an arbitrary point $p(\xi)$ on the beam reference line is identified uniquely by means of an abscissa $\xi \in B$. The equilibrium equation of the beam is stated in terms of internal forces and moments ϑ and external (imposed) loads τ:

$$\vartheta' - T^T \vartheta + \tau = 0 \tag{1}$$

where the prime denotes differentiation with respect to ξ and the matrix T is defined as

$$T = \begin{bmatrix} 0 & p'\times \\ 0 & 0 \end{bmatrix}$$

and represents the moment arm of the internal force ϑ in the differential equilibrium equation of the moments. This result follows from the axiomatic assumption according to which the density of strain power caused by a rigid motion vanishes. The operator $(\cdot)\times$ represents the vector product matrix. (If a, b are two vectors, $a\times$ is the matrix that multiplies b to give $a \times b$.) Internal forces are related to deformations by means of a constitutive law. Under the assumption that the strains remain small even when the structure undergoes large displacements and rotations, the components of ψ can be related to the internal forces and moments ϑ by means of a linear elastic constitutive law, i.e.,

$$\vartheta = D\psi \tag{2}$$

where D plays the role of an arbitrary sectional stiffness matrix. (The only constraint is due to the consideration that when a purely elastic constitutive law is considered it must be able to represent a conservative strain energy.) The proposed formulation can be extended in a straightforward manner to the case of an arbitrary constitutive law. However, when there are excursions beyond the linear elastic range, the beam model may not apply, and an extended analysis of local nonlinear constitutive phenomena is required. References 1 and 4 present a semi-analytical formulation based on the discretization of the beam section in a finite element sense. This formulation allows numerical determination of the coefficients of the linear elastic constitutive law for fully anisotropic, nonhomogeneous beam sections, thus allowing a wide variety of nonconventional beams to be modeled.

Finite Equilibrium: Weighted Residuals Interpretation

The finite volume approach can be interpreted, in a mathematical sense, as a weighted-residuals weak formulation of the equilibrium of a finite portion of the beam. Equation (3) is a weak form of Eq. (1), from which it can be derived in a straightforward way:

$$\int_a^b w(\vartheta' - T^T\vartheta + \tau)\,\mathrm{d}\xi = 0 \tag{3}$$

The weight function $w = \mathrm{step}(\xi - a) - \mathrm{step}(\xi - b)$ assumes a value of unity inside the domain $[a, b]$. The function w has the following properties:

$$\left.\begin{matrix} w = 0 \\ w' = 0 \end{matrix}\right\}\xi = [-\infty, a^-], \quad \xi = [b^+, +\infty], \qquad \left.\begin{matrix} w = 1 \\ w' = 0 \end{matrix}\right\}\xi = [a^+, b^-]$$

$$\left.\begin{matrix} w = \frac{1}{2} \\ w' = \infty \end{matrix}\right\}\xi = a, \qquad \left.\begin{matrix} w = \frac{1}{2} \\ w' = -\infty \end{matrix}\right\}\xi = b$$

$$\int_{-\infty}^{\infty} fw'\,\mathrm{d}\xi = f(a) - f(b)$$

that is, $w' = \delta(\xi - a) - \delta(\xi - b)$, where δ is the Dirac impulse function. Integrating by parts, Eq. (3) yields the following finite equilibrium relationship:

$$\left(I - \int_{\xi_0}^{\xi} T^T\,\mathrm{d}\eta\right)\vartheta\Big|_a^b = -\int_a^b w\left(I - \int_{\xi_0}^{\xi} T^T\,\mathrm{d}\eta\right)\tau\,\mathrm{d}\xi \tag{4}$$

where ξ_0 corresponds to the arbitrary pole to which the moments are referred. In a heuristic sense the finite volume approach directly describes the equilibrium of a finite section of a beam. In fact Eq. (4) states that the internal forces at the ends of the beam section under analysis must balance the sum of all of the external loads. Concentrated loads can be easily taken into account by means of Dirac functions in distributed loads τ. The integration of matrix T gives

$$\int_{\xi_0}^{\xi} T\,\mathrm{d}\xi = \begin{bmatrix} 0 & [p(\xi) - p(\xi_0)]\times \\ 0 & 0 \end{bmatrix} = U(\xi) - U(\xi_0)$$

which represents the moment arm of internal and imposed forces when contributing to the equilibrium equation of the moments. Equation (4) can be written as

$$[I - U^T(\xi)]\vartheta|_a^b = -\int_a^b w\left[I - U^T(\xi) + U^T(\xi_0)\right]\tau\,\mathrm{d}\xi \tag{5}$$

The points that bound the arbitrary finite beam section have been called evaluation points.[14] The internal forces of the beam are evaluated only at these points; this greatly simplifies the equilibrium equations. Equation (5) really is an equilibrium equation in terms of forces and couples, and thus could be written directly without any mathematical interpretation. The left-hand side of Eq. (5) represents the contribution of the internal forces at the ends a, b of the finite volume, whereas the right-hand side is the contribution of the external loads. Symmetry is lost because of the moment arm matrix U that premultiplies the internal forces. When the dependence of the internal forces on the strains is expressed by means of the linear constitutive law in Eq. (2), a finite equilibrium equation in terms of strains and curvatures at the evaluation points can be explicitly written, leading to the usual stiffness matrix of the finite beam in the linear case. In fact, the finite volume approach can be seen to be a more formal framework among the many classical lumping and finite difference methods for the analysis of beams. Its introduction here is significant expecially in view of its use in large displacement multibody analysis.

Generalized Strains

The generalized strains can be expressed in terms of derivatives of the position and the rotation of the sections with regard to their initial configuration. The strains in the global reference frame are defined by

$$\varepsilon = p' - R\bar{p}'$$

where the rotation matrix R represents a rigid rotation from the initial configuration of an arbitrary section. Overlined quantities denote the initial values of entities. Because the material constitutive matrix equation (2) does not depend on the configuration when written in the material frame, the deformations ought to be translated in that frame to obtain the proper internal forces. The strains in the material frame become

$$\tilde{\varepsilon} = R^T\varepsilon = R^T p' - \tilde{p}'$$

where the tilde $(\tilde{\cdot})$ denotes entities expressed in the material frame. The rotation deformations, i.e., the elastic curvatures, are

$$\kappa\times = R'R^T - R\tilde{\rho}\times R^T \tag{6}$$

Matrix $R'R^T = \rho\times$ is the current geometric curvature, whereas $\tilde{\rho}\times$ is the geometric curvature of the undeformed beam. The transformation from the current to the material frame leads to

$$\tilde{\kappa}\times = R^T R' - \tilde{\rho}\times = R^T\rho \times R - \tilde{\rho}\times$$

The definitions of strains and curvatures, together with the equilibrium equation, characterize the beam as a one-dimensional continuum. Thereby, the formulation is implicitly valid for initially curved and twisted beams, even if these are taken into account only in a discrete manner.

Noticeable Load Case: Inertia Forces

Inertia forces and couples represent an important load case for dynamic analyses. They express a relation between configuration, i.e., the time derivatives of the displacements, and loads, thus suggesting interesting parallels with the constitutive law. Consistent inertia loads for the proposed formulation can be easily expressed. Let the inertia loads of an arbitrary section be represented by the vector $\tau_{\text{in.}}$:

$$\tau_{\text{in.}} = -\mathcal{M}\begin{Bmatrix} \ddot{p} \\ \dot{\omega} \end{Bmatrix}$$

The contribution of the inertia of the finite piece of beam to the equilibrium equation, Eq. (5), is

$$F_{\text{in.}} = -\int_a^b \left[I - U^T(\xi) + U^T(\xi_0)\right]\mathcal{M}\begin{Bmatrix} \ddot{p} \\ \dot{\omega} \end{Bmatrix}\mathrm{d}\xi \tag{7}$$

Equation (7) shows that the finite inertia matrix is unsymmetric because the inertia forces are premultiplied by the moment arm matrix U^T.

Finite Volume Multibody Implementation

The proposed formulation has been implemented in a multibody code. Typical applications of multibody formulations can be found in the dynamics of mechanisms and large space structures. Perhaps the most challenging aeronautical application is represented by the analysis of rotorcraft. A multibody analysis program, MBDyn, has been developed at the Department of Aerospace Engineering of the Politecnico di Milano. The code is based on implicit integration of mixed algebraic and first- and second-order differential equations. It performs unconditionally A-L stable implicit integration with good accuracy. It can be classified as a Lagrangian multiplier or redundant coordinate set formulation because it uses the six position and rotation degrees of freedom of each body as unknowns, plus the internal unknown reaction forces that are related to the constraint equations. The angular velocities of each node are added as unknowns and are related to the derivatives of the rotation parameters by means of their definition, based on a rotation parameterization. As a consequence, three more degrees of freedom per body are added, the just-mentioned angular velocities, increasing the dimensions of the problem. Because the angular velocities are coupled only to the corresponding rotation parameters, there is appreciable sparsity, which is efficiently handled by means of dedicated solvers. The rotational equilibrium equations become first-order differential equations, both in the angular velocity ω and in the rotation parameters; the translational equilibrium equations are second order in the displacements.

Large Rotations

Let φ be a vector in a three-dimensional domain: $\varphi \in \Re^3$. The matrix R represents a rotation φ_Δ of the vector φ from its initial position φ_0 to a position $\varphi_1 : \varphi_1 = R\varphi_0$. Because the trigonometric functions in matrix R are costly to evaluate, the purely algebraic modified Gibbs–Rodriguez rotation parameters g are used instead of the rotational vector φ. They are defined as $g = 2n \tan(\|\varphi\|/2)$, with $n = \varphi/\|\varphi\|$, and are obtained from the usual Gibbs–Rodriguez parameters by premultiplying the factor 2. In this way, for small rotations, the parameters g coincide with the rotation vector φ. The rotation matrix is

$$R = I + \frac{4}{4 + g \cdot g}\left(g\times + \frac{1}{2} g\times g\times\right)$$

The transformation is singular for rotations that are integer multiples of angle π, but this causes no problems if an incremental solution process is used (updated Lagrangian). In this case the matrix R_0 contains the reference rotation, while the rotation unknowns are the Gibbs parameters that represent the incremental rotation R_Δ from the reference configuration R_0 to the new one R_1 at the end of the current integration step. The difference between the two configurations is assumed to be sufficiently small for an acceptable accuracy, so that no singularity should results. The kinematic unknowns of an arbitrary node and their time derivatives are

$$q = \begin{Bmatrix} x \\ g \\ \omega \end{Bmatrix}, \qquad \dot{q} = \begin{Bmatrix} \dot{x} \\ \dot{g} \\ \dot{\omega} \end{Bmatrix}, \qquad \ddot{q} = \begin{Bmatrix} \ddot{x} \\ 0 \\ 0 \end{Bmatrix}$$

where the x are the Cartesian positions of the node, g are the parameters describing the incremental, finite rotation from the last completed iteration to the current iteration, and ω are the angular velocities of the point, defined as $w = G\dot{g}$, where

$$G = \frac{4}{4 + g \cdot g}\left(I + \frac{1}{2} g\times\right) \tag{8}$$

There are six equilibrium equations and three equations relating the angular velocities to the time derivatives of the rotation parameters, for a total of nine equations for every body. Constraint equations add reaction unknowns. The resulting system of equations is differential algebraic (DAE) of index three[17] and is solvable to the desired accuracy under relatively loose conditions.

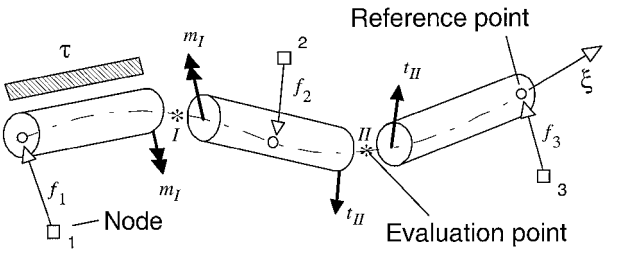

Fig. 1 Finite volume three-node beam.

Finite Volume Multibody Beam Element

The proposed finite volume beam element has been developed to give the code the capability to model the elastic deformation of bodies undergoing large displacements and rotations. According to the philosophy of the program, deformable beams can be interpreted as discrete elastic constraints that link independent rigid bodies. The finite volume approach proved to be suitable for the multibody formulation, because it leads to collocated evaluation of the elastic forces, as opposed to rather more sophisticated variational methods that require the (numerical) integration of some energy quantity.[13] A computation for a three-node beam element has been implemented, which is sketched in Fig. 1. This problem has been chosen because in the linear case, with a proper choice of the evaluation points, the element gives an exact solution for loads applied at the ends.[14] A piece of beam is divided in three parts that are related to three reference points, i.e., the midpoint and the two endpoints. They are related to geometrical nodes by means of offsets f. This allows the elastic axis of the beam to be offset from its center of mass. Every node is characterized by a position vector and a rotation matrix. A reference line p describes the position of an arbitrary point $p(\xi)$ on the beam section; the configuration of the section at an arbitrary location ξ is described by a rotation matrix $R(\xi)$. The reference line is not required to have some physical significance (e.g., the center of axial stresses). The direction e_1 of the section reference frame is normal to the section; directions e_2, e_3 are mutually orthogonal, are normal to e_1, and lie in the section plane. The angle between the unit vector e_1 and the reference line represents the shear strain. The effects of cross-section warping are assumed to be small and are neglected.[7]

Generalized Deformations

The beam generalized strains have already been defined. In the spirit of the just-mentioned updated Lagrangian approach to the rotations, the curvatures can be expressed in terms of updated rotation parameters g_Δ, as follows in a straightforward manner from the derivation of matrix R, Eq. (6):

$$\kappa\times = (Gg'_\Delta)\times + R_\Delta \kappa_r \times R_\Delta^T$$

From now on, the subscript Δ will be discarded from the incremental rotation parameters. The matrix R_Δ represents the variation of rotation matrix that occurs during the running iteration, namely $R = R_\Delta R_r$. Only the matrix R_Δ depends on the rotation parameters g, whereas the vector κ_r and the matrix R_r, respectively, represent the curvature and the rotation matrix at the last completed time step. Matrix G is defined in Eq. (8) and depends on the finite rotation from the reference frame at the last iteration to that at the current iteration. In the material frame the elastic curvatures are

$$\tilde{\kappa} = R^T G g' + \tilde{\kappa}_r$$

and only the first addendum on the right-hand side depends on the unknown rotation parameters g, both in the matrices R and G and in the vector g'.

Equilibrium

The nodal equilibrium equations are summarized as follows:

$$\mathcal{A}\mathcal{D}\Psi = \mathcal{F} \tag{9}$$

where $\mathcal{A}$ is the so-called moment arms matrix; the matrix $\mathcal{D}$ is block diagonal and contains the constitutive matrices of the sections at the

evaluation points, expressed in the global frame; vector Ψ represents the generalized deformations at the just-mentioned points. Vector $\mathcal{F}$ represents the imposed nodal loads. Roman and Arabic subscripts denote entities related to the two evaluation points and the three nodes of a beam element, respectively. The matrices take the form

$$\mathcal{A} = \begin{bmatrix} -I & 0 & 0 & 0 \\ (p_I - x_1)\times & -I & 0 & 0 \\ I & 0 & -I & 0 \\ -(p_I - x_2)\times & I & (p_{II} - x_2)\times & -I \\ 0 & 0 & I & 0 \\ 0 & 0 & -(p_{II} - x_3)\times & I \end{bmatrix} \tag{10}$$

The variables p, having Roman subscripts, are the positions of the evaluation points, and the variables x, having Arabic subscripts, are the positions of the reference points of the beam. The matrix $\mathcal{A}$, Eq. (10), directly follows from finite equilibrium, Eq. (5), where the left-hand matrix U has been evaluated at points p_I, p_{II}, assuming as reference the positions of the nodes. The constitutive matrix is known in the material reference frame and must be transformed in the current frame of each section. This can be accomplished by means of a generalized rotation matrix $\mathcal{R}$:

$$\mathcal{D} = \mathcal{R}\tilde{\mathcal{D}}\mathcal{R}^T$$

Matrix $\mathcal{R}_{(12\times 12)}$ is block diagonal, i.e.,

$$\mathcal{R} = \mathrm{diag}([R_I \quad R_I \quad R_{II} \quad R_{II}])$$

Matrices R_I, R_{II} are the rotation matrices at the evaluation points. The left multiplying $\mathcal{R}$ matrix accounts for the transformation of internal forces at the evaluation points from the beam sections to the global reference frame. The right multiplying $\mathcal{R}$ matrix accounts for the transformation of the generalized deformations at the evaluation points from the global to the beam-section reference frame. Matrix $\tilde{\mathcal{D}}$ is

$$\tilde{\mathcal{D}} = \begin{bmatrix} \tilde{D}_I & 0 \\ 0 & \tilde{D}_{II} \end{bmatrix} \tag{11}$$

where $\tilde{D}_I$, $\tilde{D}_{II}$ are the 6×6 constitutive matrices at the evaluation points in the material reference frame. Generalized strains and curvatures are

$$\Psi = \{\varepsilon_I \quad \kappa_I \quad \varepsilon_{II} \quad \kappa_{II}\}^T$$

The external loads vector is

$$\mathcal{F} = \begin{Bmatrix} \int_{\xi_1}^{\xi_I} [I - U^T(\xi) + U^T(\xi_1)]\tau \, \mathrm{d}\xi \\ \int_{\xi_I}^{\xi_{II}} [I - U^T(\xi) + U^T(\xi_2)]\tau \, \mathrm{d}\xi \\ \int_{\xi_{II}}^{\xi_3} [I - U^T(\xi) + U^T(\xi_3)]\tau \, \mathrm{d}\xi \end{Bmatrix}$$

and can be briefly indicated as $\mathcal{F} = \{F_1 \;\; C_1 \;\; F_2 \;\; C_2 \;\; F_3 \;\; C_3\}^T$.

Discretization

The position of the ith reference point is $p_i = x_i + R_i \bar{f}_i$, where x_i is the position of the ith node, R_i is its rotation matrix, and $\bar{f}_i$ is the offset in the node reference frame. The position of an arbitrary point of the reference line is interpolated from the positions of the nodes by means of parabolic shape functions $N(\xi)$:

$$p(\xi) = N_i(\xi)(x_i + R_i \bar{f}_i) \tag{12}$$

where subscript i refers to the ith node and summation over repeated indices is assumed. The shape functions are

$$N(\xi) = [1/2\xi(\xi - 1) \quad 1 - \xi^2 \quad 1/2\xi(\xi + 1)]$$

Rotation parameters g are discretized using the same shape functions:

$$g(\xi) = N_i(\xi) g_i$$

The generalized deformations at an arbitrary point are

$$\varepsilon(\xi) = N_i'(\xi)(x_i + R_i \bar{f}_i) - R(\xi)\bar{p}'$$

$$\kappa(\xi) = G(\xi) N_i'(\xi) g_i + R_\Delta(\xi)\kappa_r$$

Linearization of the Equilibrium Equations

The solution of the system requires local linearization of the equations with respect to the unknowns, i.e., the nodal position and rotation unknowns Δx_i and Δg_i. The following relations hold:

$$\Delta x_J = N_{Jk}\Delta x_k$$

$$\Delta g_J = N_{Jk}\Delta g_k$$

$$\Delta R_J = [(G_J N_{Jk}\Delta g_k)\times](R_r)_J$$

$$\Delta p_J = N_{Jk}\{\Delta x_k - [(R_r \bar{f})_k \times] G_k \Delta g_k\}$$

$$\Delta \tilde{\varepsilon}_J = (R_r)_J^T (p_J' \times) G_J N_{Jk}\Delta g_k + R_J^T N_{Jk}'\{\Delta x_k - [(R_r \bar{f})_k \times] G_k \Delta g_k\}$$

$$\Delta \tilde{\kappa} = (R_r)_J^T [(G_J g_J')\times] G_J N_{Jk}\Delta g_k + R_J^T [H(g_J') N_{Jk}\Delta g_k + G_J N_{Jk}'\Delta g_k]$$

where subscript J denotes the Jth evaluation point, whereas subscript k denotes the kth node. The matrix H follows from the relation $\Delta(Gg') = \Delta G g' + G\Delta g'$ and represents the differentiation of matrix G, such that $H(g')\Delta g = \Delta G g'$:

$$\Delta G g' = \frac{2}{4 + g \cdot g}(-g \cdot \Delta g G + \Delta g \times) g'$$

$$= -\frac{2}{4 + g \cdot g}[(Gg') \otimes g + g' \times]\Delta g$$

The linearization of Eq. (9) gives

$$\Delta\mathcal{A}\Theta + \mathcal{A}\Delta\Theta + \mathcal{A}\Theta = 0$$

Differentiation of matrix $\mathcal{A}$ is straightforward and involves the distance between the evaluation points p_I, p_{II} and the nodes of the beam:

$$\Delta\mathcal{A}_{iJ}\vartheta_J = \begin{Bmatrix} 0 \\ -t_J \times (\Delta p_J - \Delta x_i) \end{Bmatrix}$$

Differentiation of the internal forces gives

$$\Delta\vartheta_J = -\begin{Bmatrix} (t_r)_J \times \\ (m_r)_J \times \end{Bmatrix} G_J \Delta g_J + \begin{bmatrix} R_J & 0 \\ 0 & R_J \end{bmatrix} \tilde{D}_J \begin{Bmatrix} \Delta\tilde{\varepsilon}_J \\ \Delta\tilde{\kappa}_J \end{Bmatrix}$$

where the differentiation of strains and curvatures has already been defined. These elastic terms contribute to the already outlined multibody dynamic system, which already accounts for the contribution of lumped inertia. The consistent (i.e., distributed) inertia forces require numerical integration. Their linearization is not reported in this paper because it has not been implemented yet. For the sake of completeness, the external loads should be linearized, too, because the deformation of the beam changes the moment arm of the forces, i.e., the matrix U, on the right-hand side of the equilibrium equation. This effect vanishes when only forces applied at the nodes are considered.

Important Simplification: Linear Case

The important case of the linear finite volume beam is obtained by linearizing the strains and the curvatures only. The linear deformations are

$$\varepsilon = p' + p'_0 \times \varphi, \qquad \kappa = \varphi' \tag{13}$$

where φ represents the linearized rotation. The linearized modified Gibbs parameters coincide with the rotation vector. The finite equilibrium equation, Eq. (9), becomes

$$\begin{bmatrix} -I & 0 & 0 & 0 \\ -(p_I - x_1)\times & -I & 0 & 0 \\ I & 0 & -I & 0 \\ (p_I - x_2)\times & I & -(p_{II} - x_2)\times & -I \\ 0 & 0 & I & 0 \\ 0 & 0 & (p_{II} - x_3)\times & I \end{bmatrix} \mathcal{D} \begin{Bmatrix} \varepsilon_I \\ \kappa_I \\ \varepsilon_{II} \\ \kappa_{II} \end{Bmatrix} = \begin{Bmatrix} F_1 \\ C_1 \\ F_2 \\ C_2 \\ F_3 \\ C_3 \end{Bmatrix} \tag{14}$$

Discretization of Eqs. (13) is straightforward:

$$\varepsilon = N'_i x_i + p'_0 \times N_i \varphi_i - N'_i f_i \times \varphi_i, \qquad \kappa = N'_i \varphi_i$$

The linear finite equilibrium relation Eq. (14) can be written in form of the usual linearized stiffness matrix:

$$\mathcal{A}\mathcal{D} \begin{bmatrix} N'_{Ii} & (p'_{0I} \times N_{Ii} - N'_{Ii} f_i \times) \\ 0 & N'_{Ii} \\ N'_{IIi} & (p'_{0II} \times N_{IIi} - N'_{IIi} f_i \times) \\ 0 & N'_{IIi} \end{bmatrix} \begin{Bmatrix} x_i \\ \varphi_i \end{Bmatrix} = \mathcal{F}$$

Matrices $\mathcal{A}$ and $\mathcal{D}$, offsets f_i, and the initial derivatives of the position p'_{0I} and p'_{0II} are the same as in the general formulation; they are evaluated in the reference configuration and do not participate in the linearization.

Numerical Results

Static Load of a Cantilever Beam

The proposed beam element formulation is able to determine the exact solution in terms of nodal displacements and internal forces when loaded at its ends. Consider directly the case of a transverse unit load applied to the free end of a clamped beam in the direction y. The exact solution for a linear C^0 beam with constant properties is

$$p_y = \tfrac{1}{2}(l/GA)(\xi + 1) + \tfrac{1}{48}(l^3/EJ)(5 + 9\xi + 3\xi^2 - \xi^3)$$

$$\varphi_z = \tfrac{1}{8}(l^2/EJ)(3 + 2\xi - \xi^2)$$

where l is the length of the beam, EJ and GA are the bending and shear stiffnesses, and ξ is a nondimensional abscissa ranging from -1, at the clamped end, to 1, at the free end. The proposed formulation uses second-degree shape functions for both the displacement and the rotation; the interpolated shear strain $\gamma = p'_y - \varphi_z$ due to the exact nodal values is

$$\gamma = (1/GA) + \tfrac{1}{24}(l^2/EJ)(3\xi^2 - 1) \tag{15}$$

The exact value for the shear strain $\gamma = 1/GA$ is obtained at $\xi = \pm 1/\sqrt{3}$, which are the optimal positions of the evaluation points.[14] The internal forces at these points assume their exact value, thus explaining why the exact solution for the nodal displacements is obtained. Note that the points mentioned also correspond to the exact Gauss quadrature points for second- and third-degree polynomials.

Euler Critical Load

The buckling critical load due to a conservative axial force that compresses a bar is a classical benchmark for nonlinear beam formulations. From linear elasticity theory the value of the critical load is

$$P = (\pi/2)^2(EJ/l^2)$$

for a clamped-free beam. This static stability result is correct when the axial dead load is conservative.[18] The finite volume linearized prestress matrix follows from the linearization of the moment arms matrix, Eq. (10), about an already calculated prestress condition:

$$\mathcal{F}_0 = \begin{bmatrix} 0 & 0 & 0 & 0 \\ -(p_I - x_1)\times & 0 & 0 & 0 \\ 0 & 0 & 0 & 0 \\ (p_I - x_2)\times & 0 & -(p_{II} - x_2)\times & 0 \\ 0 & 0 & 0 & 0 \\ 0 & 0 & (p_{II} - x_3)\times & 0 \end{bmatrix} \begin{Bmatrix} t_{I0} \\ m_{I0} \\ t_{II0} \\ m_{II0} \end{Bmatrix}$$

Displacements at the nodes and at the evaluation points can be easily discretized by means of Eq. (12), thus giving the following expression for the prestress stiffness matrix:

$$K_p = \begin{bmatrix} 0 & 0 \\ t_{I0} \times (N_{Ii} - \delta_1 I) & -t_{I0} \times N_{Ii} f_i \times \\ 0 & 0 \\ \begin{bmatrix} -t_{I0} \times (N_{Ii} - \delta_2 I) \\ +t_{II0} \times (N_{IIi} - \delta_2 I) \end{bmatrix} & \begin{pmatrix} t_{I0} \times N_{Ii} f_i \times \\ -t_{II0} \times N_{IIi} f_i \times \end{pmatrix} \\ 0 & 0 \\ t_{II0} \times (N_{IIi} - \delta_3 I) & -t_{II0} \times N_{IIi} f_i \times \end{bmatrix} \begin{Bmatrix} x_i \\ \varphi_i \end{Bmatrix}$$

The critical loads and the buckling shapes have been calculated for a straight, uniform beam modeled with a single element with equally spaced nodes and loaded by an axial compression force. Two buckling modes have been found in each transverse direction, whose critical values are

$$P_{\text{fv}} = 6(5 \pm \sqrt{21})(EJ/l^2) \tag{16}$$

The lower value gives an error of about 1.48%. Quasistatic simulations of the buckling condition have been performed using a slowly growing axial compression load and a small transverse load. An abrupt increase of the lateral deviation takes place when the axial load approaches the lowest critical value. Subsequently, the transverse load is removed, and if the critical value has been exceeded, the beam remains bent. The numerical simulations can only determine lower and upper bounds for the critical values because when the exact value is approached, the Jacobian matrix of the system becomes singular. The lower and upper bounds obtained by means of a single-element model exactly bound the analytic value given by Eq. (16). The bounds obtained using a four-element model are correct to within $\pm 0.04\%$, showing the effectiveness of a relatively coarse model. The beam can resist a load that is larger than the critical load when the full nonlinear behavior is taken into account, but a large curvature develops, as shown in Fig. 2. In this figure a four-element beam carries a load up to twice the buckling critical value. Figure 3 shows the internal forces at the evaluation points due to the two P_{cr} load.

Dynamics of a Helicopter Rotor Blade

This example deals with the analysis of the dynamics of a rotor blade. The model represents the rotor blade of a commercial helicopter. The blade is made of a C-shaped aluminum main spar, closed by a rear spar. The whole structure is covered by an aluminum sheet and represents about one-third of the chord. The trailing part of the airfoil is honeycombed, and it is covered by an aluminum skin. The trailing edge is made of a V-shaped aluminum rib. A steel antiabrasive strip is put on the leading edge. Nonstructural masses have been also taken into account, as well as glue and paint weight. Fourteen cross sections of the blade have been analyzed by means of a dedicated finite element code.[1,4] The spars and the honeycomb have been modeled by means of brick elements, whereas two-dimensional laminæ have been used for the skin and the antiabrasive strip. A three-dimensional model was then generated, made of 15 three-node beam elements (Fig. 4). A modal analysis of the model has been performed using a linear finite volume beam model. Both concentrated and consistent inertia forces have been used to determine the influence of a less refined model on the results of the analysis. Then the frequency response function (FRF) of the blade has been calculated by analysing the power spectral density (PSD)

of the blade excited with a random force at one end. The response has been computed by means of the multibody code, using the same model of the linear analysis. The results of the spectral analyses are reported in Table 1. The modal frequencies obtained by means of the PSD of the response computed with the multibody code are in a good agreement with the experiment and with other analyses.

Ground Resonance of an Elastic Windmill

Description

An elastic tower 7.5 m high carries a gear fairing 1 m long, on which a three-blade articulated rotor is mounted. The inertial and stiffness properties of the system are summarized in Table 2. The tower carries a 50-kg concentrated mass. The rotor hub is represented by a 20-kg mass and rotates about a revolution hinge, having a horizontal axis, at the free end of the fairing. The three blades are mounted on the hub with a 0.25-m offset. They can freely rotate about the flap and lag hinges that are coincident; the pitch is imposed. The blades span 5 m; both rigid and deformable blades have been considered. The tower is modeled with two three-node beam elements. One element is used for the fairing. Both the tower and the fairing have the same elastic and inertial properties. The internal forces are output at the first evaluation point of the first beam element, that is, at 0.792 m from the base of the tower. Each deformable blade is modeled with two beam elements. The blade elastic and inertial properties are constant spanwise. Aerodynamic loads on the blades are based on the strip theory and assume uniform inflow. The blades have a constant spanwise chord of 0.25 m. A simple NACA 0012 airfoil with experimentally determined aerodynamic coefficients spanning 360 deg of angle of attack is considered. Standard air density at zero altitude is considered, that is, $\rho = 1.225\,\mathrm{kg/m^3}$. Hyperbolic twisting is imposed to obtain a spanwise uniform inflow angle. Two half-span aerodynamic elements per blade are considered. The same aerodynamic discretization has been used for both the rigid and the deformable blades. The twist is modeled by means of parabolic interpolation along each aerodynamic element.

Table 1 Frequencies of a helicopter rotor blade

Mode	Mode type	Exper.	Ref. 12	Lumped	Consist.
1	1 Beam	7.42	7.49	7.49	7.49
2	2 Beam	21.90	21.93	21.91	21.89
3	3 Beam	42.55	43.17	42.72	42.88
4	1 Chord	43.36	44.45	44.51	44.47
5	1 Torsional	65.70	66.35	68.32	66.22
6	4 Beam	70.81	73.34	72.64	72.62
7	5 Beam	105.78	110.20	107.51	107.85
8	2 Chord	121.97	125.34	125.69	125.57

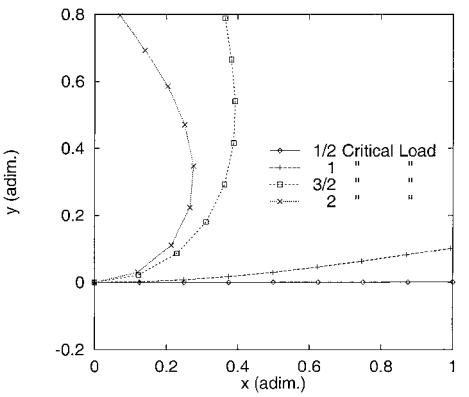

Fig. 2 Deformed shapes of a four three-node element beam under 1, $\frac{3}{2}$, and 2 times the critical buckling load.

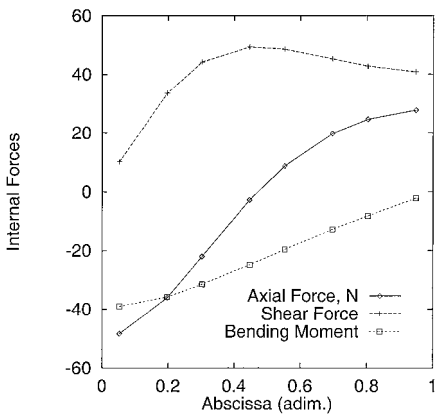

Fig. 3 Internal forces due to twice the critical buckling load, at the evaluation points of the four-beam element model.

Assessment of the Integration

The first two simulations were made in vacuo; the rigid blade rotor had initial speeds of 20 and 30 rad/s, respectively, to which stable and ground resonance conditions correspond. To check the stability of the system, the rotating speed of blade #1 was slightly perturbed ($\Delta\Omega = -0.01$ rad/s). As a consequence, the center of gravity of the rotor moves from the rotation axis. In the first case the system responds with slightly damped but stable in-plane oscillations, as shown in Fig. 5, which shows the moments in the tower.

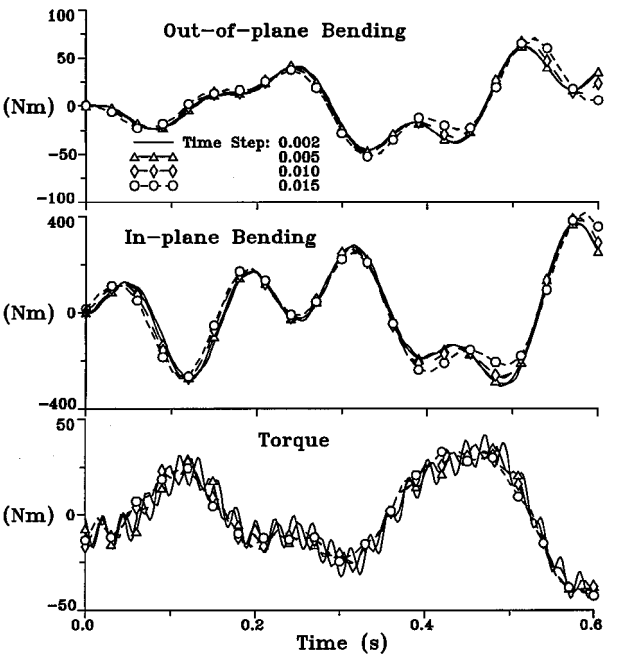

Fig. 5 Windmill: internal forces in the tower, in vacuo stable case (Ω = 20 rad/s).

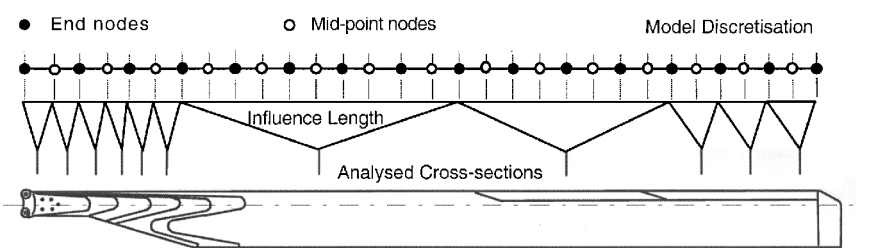

Fig. 4 Sketch of the discretized helicopter blade.

Table 2 Properties of the windmill

Component	Stiffness, N			Stiffness, N · m			Mass kg/m
	Axial	Shear, 2	Shear, 3	Torsional	Bending, 2	Bending, 3	
Tower	1.0×10^6	1.0×10^9	1.0×10^9	2.0×10^7	4.0×10^7	4.0×10^7	12.0
Fairing	1.0×10^6	1.0×10^9	1.0×10^9	2.0×10^7	4.0×10^7	4.0×10^7	12.0
Blades	1.0×10^6	1.0×10^7	1.0×10^6	1.0×10^6	1.0×10^5	1.0×10^4	3.0

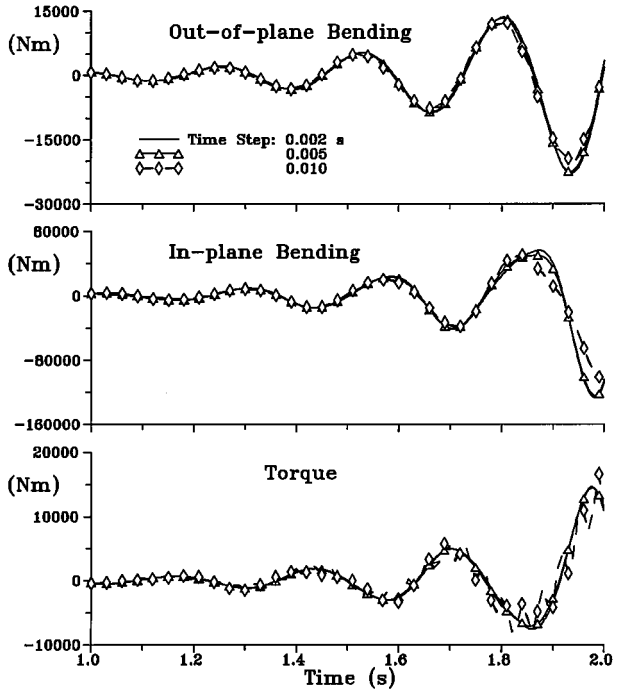

Fig. 6 Windmill: internal forces in the tower, in vacuo unstable case (Ω = 30 rad/s).

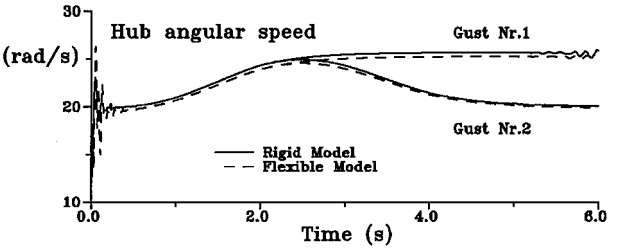

Fig. 7 Windmill: velocity of the hub, in-air unstable and stability recovery cases (gusts #1 and #2).

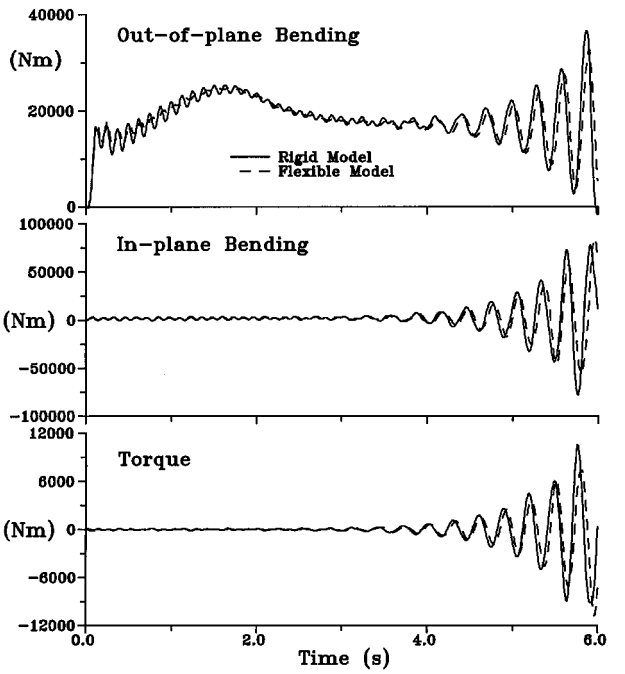

Fig. 8 Windmill: internal moments in the tower, in-air unstable case (gust #1).

In the second case the system is unstable, and the diverging unstable motion is apparent from the internal moments in the tower, as shown in Fig. 6. All of the simulations were performed with a time step of 0.005 s. Slight numerical damping is added by means of a linearly *A*-stable implicit time-step integrator that allows the user to impose the desired asymptotic value of the spectral radius. A value of 0.6 is used unless otherwise stated. Trials were run to assess the effects of the time step and the numerical damping on the results. Time steps up to 0.015 s have been tested, which resulted in little loss in accuracy in the unstable case when low numerical damping was used, i.e., $\rho_\infty = 0.6$. In the case of high numerical damping, the accuracy is good at a time step of 0.002 s but much poorer at 0.02 s. For time steps of 0.002 s, 0.005 s, and 0.01 s, the differences in the overall motion are quite slight, the more appreciable errors being in the high-frequency motions that are negligible in ground resonance. Only for a time step of 0.015 s is the overall motion considerably distorted. The internal forces in Fig. 5 strongly depend on the time step for the high-frequency motion, the largest errors being caused mainly by the period distortion caused by the numerical integration. Again, only for the 0.015 s time step are the high-frequency internal forces appreciably distorted. The unstable motion depicted in Fig. 6 is clearly dominated by the retreating lag-frequency motion (in the fixed frame); it is correctly modeled with time steps up to 0.01 s when low numerical damping is considered (asymptotic value of the spectral radius of 0.6). When a 0.015 s or larger time step is considered, or when the spectral radius is smaller than 0.3 with a time step of 0.01 s or larger, the response is appreciably different from the baseline. Based on these results, the selected time step and numerical damping are adequate for the spectrum of the system under analysis.

Ground Resonance with Aerodynamic Loads

Subsequent simulations involved the presence of an airstream. In the third case the simulation starts with the rotor at a stable speed of 20 rad/s, and a steady axial airstream speed of 20 m/s is applied. The collective pitch of the blades is set at 2 deg, corresponding to an aerodynamic torque of about 1600 Nm. A corresponding reacting torque is applied at the rotor shaft. Initial oscillations caused by the untrimmed initial conditions can be seen in Fig. 7. They are quickly damped by the aerodynamic forces. During this transient phase, the rotor blades assume the correct steady cone and lag angles. The tower and the fairing bend and twist under the net traction and the torque of the rotor, resulting in a displacement of the rotor center. Then, in 2 s, the airstream is raised to 25 m/s, which causes the rotor to reach an unstable rotation speed of about 25 rad/s. The internal moments are plotted in Fig. 8, whereas the diverging motion can be seen in Fig. 9, which shows the path of the hub in the plane of the rotor. If the airstream speed is immediately put back at 20 m/s (fourth case), the stable motion is restored. Figure 10 shows the internal moments; Fig. 11 shows the flapping and the lead-lag angles, and the recovery of stable conditions can be clearly seen. Figure 7 shows the hub rotation velocity vs time related to the two perturbed simulations for both the rigid and the deformable blade rotor. Because the rigid and the deformable blades share the same aerodynamic discretization, the slight differences in their response are caused by the aeroelastic effects that occur in the flexible model.

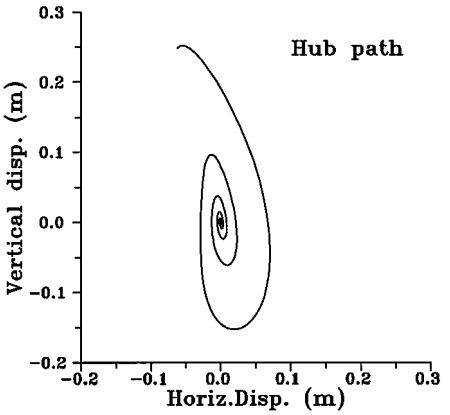

Fig. 9 Windmill: path of the hub, in-air unstable case (gust #1).

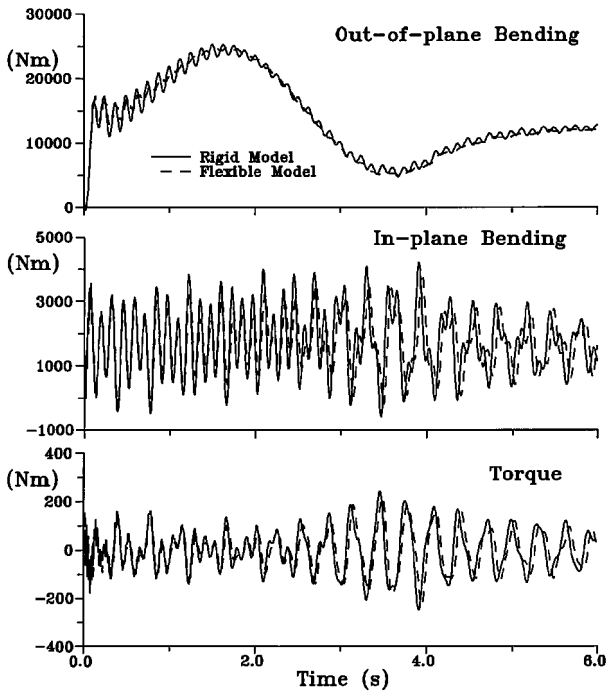

Fig. 10 Windmill: internal moments in the tower, in-air stability recovery case (gust #2).

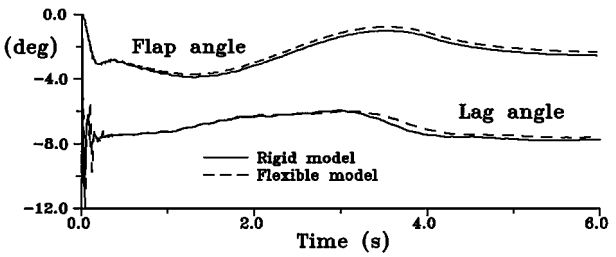

Fig. 11 Windmill: flap and lead-lag angles, in-air stability recovery case (gust #2).

All of the simulations start abruptly at the nominal rotation speed, with both aerodynamic and inertial loads applied to the initially unloaded structure. To suppress high-frequency axial oscillations in the flexible blades, physical damping in axial direction only is added by means of the following viscoelastic constitutive law $\vartheta = D\psi + E\dot{\psi}$, where $\dot{\psi}$ are the time derivatives of the generalized strains. In this way, the initial oscillations are damped in less than 0.2 s, with no appreciable loss in accuracy.

Concluding Remarks

A new, easy to implement, computationally efficient beam formulation has been proposed, based on the finite volume concept. The formulation has a strong physical basis because it can be directly developed from the equilibrium equations of a finite beam. The formulation has been applied to arbitrarily curved and twisted beams undergoing finite displacements and rotations. Finite volumes are used to form the equilibrium equations of the finite beam. Internal forces must be evaluated only at the boundaries of the volumes, thus simplifying their contribution to the equilibrium equations. Consistent inertia forces have been considered, as well as prestress conditions, in both the linear (linearized) and nonlinear cases. A multibody implementation has been described in detail. The proposed implementation gives considerable freedom in analysis, by defining offsets from the reference points of the beam to the physical degrees of freedom, and independent reference frames for the beam sections in which the forces are calculated. One drawback, the loss of symmetry in the stiffness matrix, is not crucial in sophisticated, nonlinear, and intrinsically nonsymmetric problems, such as aeroservoelastic analyses. Consistent instead of lumped inertia should be used if a coarse model is to be considered. Some classical benchmarks, along with more sophisticated problems, such as modal analysis and nonlinear time-step simulations of real models, have been presented to demonstrate the soundness of the formulation.

References

[1]Giavotto, V., Borri, M., Mantegazza, P., Ghiringhelli, G. L., Caramaschi, V., Maffioli, G. C., and Mussi, F., "Anisotropic Beam Theory and Applications," *Computers and Structures*, Vol. 16, No. 1–4, 1983, pp. 403–414.

[2]Bauchau, O. A., "A Beam Theory for Anisotropic Material," *Journal of Applied Mechanics*, Vol. 52, No. 2, 1985, pp. 416–422.

[3]Hodges, D. H., Atilgan, A. R., Cesnik, C. E. S., and Fulton, M. V., "On a Simplified Strain Energy Function for Geometrically Non Linear Behaviour of Anisotropic Beams," *Composites Engineering*, Vol. 2, Nos. 5–7, 1992, pp. 513–516.

[4]Ghiringhelli, G. L., and Mantegazza, P., "Linear, Straight and Untwisted Anisotropic Beam Section Properties from Solid Finite Elements," *Composites Engineering*, Vol. 4, No. 12, 1994, pp. 1225–1240.

[5]Borri, M., Ghiringhelli, G. L., and Merlini, T., "Linear Analysis of Naturally Curved and Twisted Anisotropic Beams," *Composites Engineering*, Vol. 2, No. 5–7, 1992, pp. 433–456.

[6]Bathe, K. J., and Bolourchi, S., "Large Displacement Analysis of Three-Dimensional Beams Structures," *International Journal for Numerical Methods in Engineering*, Vol. 14, No. 7, 1979, pp. 961–986.

[7]Borri, M., and Merlini, T., "A Large Displacement Formulation for Anisotropic Beam Analysis," *Meccanica*, No. 21, No. 1, 1986, pp. 30–37.

[8]Simo, J. C., "A Finite Strain Beam Formulation. The Three-Dimensional Dynamic Problem. Part I," *Computer Methods in Applied Mechanics and Engineering*, Vol. 49, No. 1, 1985, pp. 55–70.

[9]Simo, J. C., and Vu-Quoc, L., "A Three-Dimensional Finite Strain Rod Model. Part II: Computational Aspects," *Computer Methods in Applied Mechanics and Engineering*, Vol. 58, No. 1, 1986, pp. 79–116.

[10]Borri, M., and Bottasso, C., "An Intrinsic Beam Model Based on a Helicoidal Approximation—Part I: Formulation," *International Journal for Numerical Methods in Engineering*, Vol. 37, No. 13, 1994, pp. 2267–2289.

[11]Borri, M., and Bottasso, C., "An Intrinsic Beam Model Based on a Helicoidal Approximation—Part II: Linearization and Finite Element Implementation," *International Journal for Numerical Methods in Engineering*, Vol. 37, No. 13, 1994, pp. 2291–2309.

[12]Ghiringhelli, G. L., "On the Three Dimensional Behaviour of Composite Beams," *Composites Part B*, Vol. 28B, No. 5–6, 1997, pp. 613–626.

[13]Hughes, T. J. R., *The Finite Element Method*, Prentice–Hall, Upper Saddle River, NJ, 1987.

[14]Masarati, P., and Mantegazza, P., "On the C^0 Discretisation of Beams by Finite Elements and Finite Volumes," *l'Aerotecnica Missili e Spazio*, Vol. 75, No. 3–4, 1996, pp. 77–86.

[15]Ghiringhelli, G. L., Mantegazza, P., and Masarati, P., "Numerical Modelling of Anisotropic Non Homogeneous Beams with Embedded Piezoelectric Sensors and Actuators," *7th International Conference on Adaptive Structures and Technologies*, Dipartimento Aerospaziale and Facoltà di Ingegneria, Univ. of Rome "La Sapienza," Rome, 1996, pp. 24–27.

[16]Ghiringhelli, G. L., Masarati, P., and Mantegazza, P., "Multi-Body Aeroelastic Analysis of Smart Rotor Blades, Actuated by Means of Piezo-Electric Devices," *International Forum on Aeroelasticity and Structural Dynamics*, Vol. 2, Confederation of European Aerospace Societies, pp. 115–122.

[17]Brenan, K. E., Campbell, S. L., and Petzold, L. R., *Numerical Solution of Initial-Value Problems in Differential-Algebraic Equations*, North-Holland, New York, 1989, pp. 17–39, 160.

[18]Bolotin, V. V., *Nonconservative Problems of the Theory of Elastic Stability*, Pergamon, Oxford, 1963, pp. 86–134.

A. Chattopadhyay
Associate Editor